JOURNAL OF COMPUTATIONAL PHYSICS 102, 297–309 (1992)

Numerical Solution of a Free-Boundary Problem in Hypersonic Flow Theory: Nonequilibrium Viscous Shock Layers*

BRUNO LABOUDIGUE

Laboratoire EM2C du CNRS et de l'ECP, UPR 288, CNRS, Ecole Centrale Paris, 92295, Chatenay-Malabry Cedex, France

VINCENT GIOVANGIGLI

Centre de Mathématiques Appliquées, URA 756, CNRS, Ecole Polytechnique, 91128 Palaiseau Cedex, France

AND

SÉBASTIEN CANDEL

Laboratoire EM2C du CNRS et de l'ECP, UPR 288, CNRS, Ecole Centrale Paris, 92295, Chatenay-Malabry Cedex, France

Received February 16, 1990; revised July 19, 1991

Non equilibrium viscous shock layer flows produced near the stagnation point of a blunt body constitute a standard problem in hypersonic flow theory. This flow configuration is usually modeled with the viscous shock layer (VSL) equations derived by writing the full Navier–Stokes equations in boundary-layer coordinates and performing an order of magnitude analysis. The terms retained in this process assure that for moderate Reynolds numbers the resulting equations are uniformly valid between the body surface and the shock, which may be treated as a thin discontinuity. The VSL equations are generally solved by starting with the thin layer approximation (TVSL). Boundary conditions are specified at the body surface and the Rankine–Hugoniot relations are imposed at the shock. Because the position of the shock is not known, one has to solve a free boundary problem. This paper presents a novel solution procedure for this situation. A reduced coordinate is introduced and the free boundary problem is transformed into a nonlinear eigenvalue problem. The new problem for an augmented set of variables is then solved with Newton iterations and adaptive gridding. The method is illustrated in the paper with a solution of the thin shock layer equations at the stagnation streamline. The solution obtained on this line is then used as an initial condition for a two-dimensional marching procedure. The complete axisymmetric problem is solved by performing fully coupled Newton iterations; moreover, we consider a new enlarged unknown function including the shock location. The model includes detailed transport properties and complex kinetics for air dissociation and ionization. However, in order to focus on the numerical method and for the sake of simplicity, thermodynamic equilibrium is assumed.

* This research was supported by Dassault Aviation under Contract Number RDMF 86-8.

1. INTRODUCTION

The study of reentry into the Earth's atmosphere is of fundamental interest in many recent space flight projects like the trans-atmospheric airplane or the Hermes spaceplane. One of the most critical problems for the designer is that of the large rates of heat transfer and high temperatures at the nose and leading edges of the vehicle. An efficient heat protection system is needed and requires special attention. This system should be carefully designed and in particular its weight should be minimized in order to increase the payload that may be carried into orbit.

While wind-tunnel testing provides some of the data that is required to determine the aerothermodynamic environment of the thermal protection system (TPS), it is not possible to obtain a complete simulation of reentry flow conditions in ground-testing facilities. More recently, data from space shuttle flights have become available and they are being used to evaluate the performance of the protection system and verify numerical predictions. Flight data are, however, insufficient for design operations. Under these circumstances, numerical simulations of the flowfield constitute an essential tool. During the last 30 years, considerable efforts have been made to improve the computational methods and the physical models which may be used to describe the high enthalpy flows found during atmospheric reentry.

The problem of computing the hypersonic laminar flow at moderate Reynolds number past axisymmetric blunt bodies has been approached in several ways. Two of these methods

0021-9991/92 $5.00

are through the solution of first- and second-order boundary-layer equations and through numerical solution of the viscous shock layer equations. This later method is investigated in this paper. Viscous shock layer (VSL) techniques have become increasingly important with the development of parabolized Navier–Stokes (PNS) codes. This is because VSL solutions yield relatively fast and accurate blunt body solutions compared to the time consuming Navier–Stokes computations.

Early studies of viscous shock layers for hypersonic applications were conducted by, among others, Blottner [1] and Bush [2]. In addition, second-order boundary-layer effects for hypersonic flows were studied most notably by Davis and Flügge-Lotz [3]. In 1970, Davis [4] introduced a method for solving the viscous shock layer equations for a perfect gas flow. Many studies based on Davis' method and dealing with more complex physical descriptions of the flowfield (chemical non-equilibrium, wall catalycity, high-altitude effects, etc.) are available, as, for example, those of Lewis and his colleagues or Scott [5–8]. The viscous shock layer equations are derived by writing the full Navier–Stokes equations in boundary-layer coordinates and performing an order of magnitude analysis of the various terms appearing in the governing equations. The terms retained in this process assure that the resulting equations are uniformly valid between the shock and the body surface for moderate Reynolds numbers. Davis' method uses an iterative process to deal with the ellipticity of both the governing equations and the boundary conditions. The first iteration of this process consists, on one hand, in solving a simplified set of equations derived from the thin viscous shock layer approximation (TVSL). On the other hand, to remove the ellipticity of the shock boundary conditions, Davis assumed that the first derivative of the shock standoff distance with respect to the streamwise coordinate is equal to zero. This assumption means that the shock and the body surface are concentric, and hence that the shock standoff distance is constant along the body. Of course, this is not the case and this assumption is removed with successive iterations.

However, one should point out that some more recent studies as, for example, Ref. [7] do not assume a concentric shock for the first iteration. Instead a more realistic initial shock shape is calculated separately, using, for instance, an Euler code and then input to the VSL code.

In the present study, we will derive new relations at the shock by performing an order of magnitude analysis of the terms appearing in the Rankine–Hugoniot relations. Terms involving shock location second derivatives of elliptic nature are indeed eliminated, but first derivative terms are retained and included in the marching step procedure. It is thus possible to take into account realistic variations of the shock shape at the first iteration (TVSL) of the solution process. Each iteration consists of two steps. The first one comes from the specialization of the governing equations at the stagnation streamline which results in a two-point boundary value problem with a free boundary. The second one corresponds to the complete 2D marching step calculation which starts with an initial condition given by the solution on the stagnation streamline.

By introducing a reduced coordinate, the free boundary problems are transformed into non-linear eigenvalue problems. From a numerical point of view, Davis' method is based on the solution of each equation successively. However, it has been shown [9, 10] that this could lead to numerical instabilities and prevent the convergence to a solution far downstream. Waskiewicz *et al.* [10] have partly solved this problem by coupling the total mass balance and the balance of normal momentum.

In the present paper, the resulting two-point boundary value problems are solved with a method combining finite differences, fully-coupled Newton iterations, and adaptive gridding [11–15]. Pseudo-unsteady fully implicit iterations are also used in order to bring the starting estimates into the domain of convergence of Newton's method. However, no unsteady terms are appended to the coupled hydrodynamic-eigenvalue equations. The eigenvalue is also considered as a function of the transformed coordinate in order to maintain the block tridiagonal structure of the discrete equations. The usual no-slip boundary conditions are imposed at the body wall. The model includes detailed transport properties and complex kinetics for air dissociation. However, in order to focus on a novel method for solving the VSL equations, we will use a simplified physical model. It is assumed that the flow is at thermodynamic equilibrium, so that there is only one temperature at each point. To take into account ionization, we will use an air model comprising seven species (O_2, O, N_2, N, NO, NO^+, and e^-) coupled by 18 elementary reactions [16]. The simplified physical model adopted here is sufficiently realistic for a demonstration of the numerical method.

The viscous shock layer equations are presented in Section 2. The numerical method is described in Section 3 and typical numerical results are discussed in Section 4.

2. GOVERNING EQUATIONS

2.1. *Conservation Equations*

The viscous shock layer governing equations are the equations for conservation of total mass, species mass, momentum, and energy [1, 3, 4, 6, 7]. Using a local coordinate system (s, n), where s is measured along the body surface and n is normal to the body surface (see Fig. 1), the total mass conservation may be written

$$\frac{\partial \rho}{\partial t} + \frac{1}{\mathscr{H} r^j} \left\{ \frac{\partial}{\partial s} (r^j \rho u) + \frac{\partial}{\partial n} (\mathscr{H} r^j \rho v) \right\} = 0, \qquad (1)$$

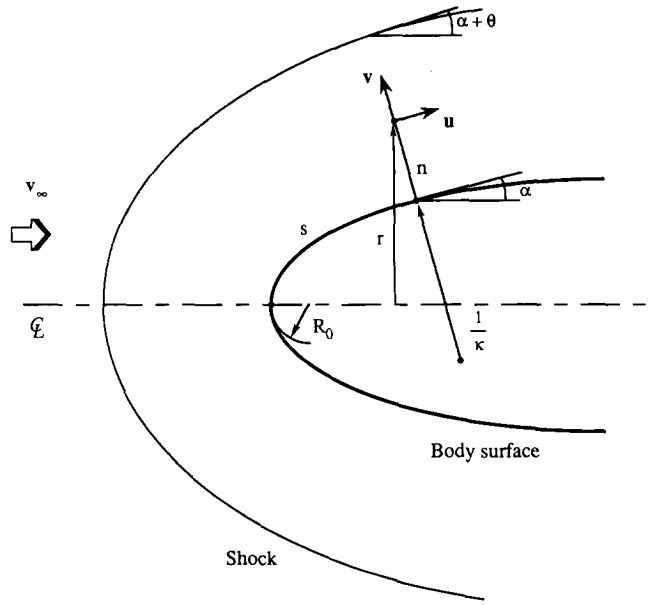

FIG. 1. Schematic of the flow configuration and the local coordinate system.

where ρ is the density, $\mathscr{H} = 1 + \kappa n$ is a curvature term, κ is the curvature of the body surface, r is the radius from the axis of symmetry, (u, v) are the mass averaged flow velocity components in the local coordinate system, t is the time. In this equation and those given below, $j=0$ and $j=1$ correspond respectively to two-dimensional and axisymmetric flows. The tangential momentum conservation equation may be written

$$\rho\frac{\partial u}{\partial t}+\frac{\rho u}{\mathscr{H}}\frac{\partial u}{\partial s}+\rho v\frac{\partial u}{\partial n}+\frac{\rho\kappa uv}{\mathscr{H}}+\frac{1}{\mathscr{H}}\frac{\partial p}{\partial s}-\frac{1}{\mathscr{H}^2 r^j}\frac{\partial}{\partial n}\left(\mathscr{H}^2 r^j\eta\left(\frac{\partial u}{\partial n}-\frac{\kappa u}{\mathscr{H}}\right)\right)=0, \tag{2}$$

where p is the pressure and η is the viscosity. The normal momentum conservation may be written

$$\rho\frac{\partial v}{\partial t}+\frac{\rho u}{\mathscr{H}}\frac{\partial v}{\partial s}+\rho v\frac{\partial v}{\partial n}-\frac{\rho\kappa u^2}{\mathscr{H}}+\frac{\partial p}{\partial n}=0. \tag{3}$$

According to the thin layer approximation [4] this equation becomes

$$-\frac{\rho\kappa u^2}{\mathscr{H}}+\frac{\partial p}{\partial n}=0. \tag{4}$$

The species mass conservation equation is

$$\rho\frac{\partial Y_k}{\partial t}+\frac{\rho u}{\mathscr{H}}\frac{\partial Y_k}{\partial s}+\rho v\frac{\partial Y_k}{\partial n}-W_k\omega_k+\frac{1}{\mathscr{H}r^j}\frac{\partial}{\partial n}(\mathscr{H}r^j\rho Y_k V_k)=0,\qquad k\in\mathscr{K}, \tag{5}$$

where Y_k is the mass fraction of the kth species, V_k is the normal component of the diffusion velocity of the kth species, W_k is the molecular weight of the kth species, ω_k is the molar production rate of the kth species, $\mathscr{K} = \{1, ..., K\}$ are the species indices, and K is the number of species. The total energy conservation may be written as

$$\rho c_p\left(\frac{\partial T}{\partial t}+\frac{u}{\mathscr{H}}\frac{\partial T}{\partial s}+v\frac{\partial T}{\partial n}\right)-\frac{\partial p}{\partial t}-\frac{u}{\mathscr{H}}\frac{\partial p}{\partial s}-v\frac{\partial p}{\partial n}-\frac{1}{\mathscr{H}r^j}\frac{\partial}{\partial n}\left(\mathscr{H}r^j\lambda\frac{\partial T}{\partial n}\right)-\eta\left(\frac{\partial u}{\partial n}-\frac{\kappa u}{\mathscr{H}}\right)^2+\sum_{k\in\mathscr{K}}\rho Y_k V_k c_{pk}\frac{\partial T}{\partial n}+\sum_{k\in\mathscr{K}}h_k W_k\omega_k=0, \tag{6}$$

where T is the temperature, c_p is the constant pressure heat capacity of the mixture, c_{pk} is the constant pressure heat capacity of the kth species, λ is the thermal conductivity of the mixture, and h_k is the specific enthalpy of the kth species.

2.2. *Equations along the Stagnation Streamline* $s = 0$

In order to obtain the steady governing equations along the stagnation streamline, all the dependent variables ϕ are expanded near $s = 0$ in the form

$$\phi(s, n) = s^{i_\phi}(\bar{\phi}(n) + s^2\tilde{\phi}(n) + O(s^4)), \tag{7}$$

where the index i_ϕ is zero except for the polar radius r and the u velocity component for which $i_r = i_u = 1$. Substitution of these expansions into the governing equations leads to the following two-point boundary value problem with a free boundary. The conservation equations become

$$\frac{1+j}{\bar{\mathscr{H}}}\rho\bar{u}+\frac{1}{\bar{\mathscr{H}}^{(1+j)}}\frac{d}{dn}(\bar{\mathscr{H}}^{(1+j)}\bar{\rho}\bar{v})=0, \tag{8}$$

$$\frac{1}{\bar{\mathscr{H}}}\bar{\rho}\bar{u}^2+\bar{\rho}\bar{v}\frac{d\bar{u}}{dn}+\frac{\bar{\rho}\kappa\bar{u}\bar{v}}{\bar{\mathscr{H}}}+\frac{2}{\bar{\mathscr{H}}}\tilde{p}-\frac{1}{\bar{\mathscr{H}}^{(2+j)}}\frac{d}{dn}\left(\bar{\mathscr{H}}^{(2+j)}\eta\left(\frac{d\bar{u}}{dn}-\frac{\kappa\bar{u}}{\bar{\mathscr{H}}}\right)\right)=0, \tag{9}$$

$$\frac{d\bar{p}}{dn}=0, \tag{10}$$

$$-\frac{\bar{\rho}\kappa\bar{u}^2}{\bar{\mathscr{H}}}+\frac{d\tilde{p}}{dn}=0, \tag{11}$$

$$\bar{\rho}\bar{v}\frac{d\bar{Y}_k}{dn}-W_k\omega_k+\frac{1}{\bar{\mathscr{H}}^{(1+j)}}\frac{d}{dn}(\bar{\mathscr{H}}^{(1+j)}\bar{\rho}\bar{Y}_k\bar{V}_k)=0,\qquad k\in\mathscr{K}, \tag{12}$$

$$\bar{\rho}\bar{v}\bar{c}_p\frac{d\bar{T}}{dn}-\frac{1}{\bar{\mathscr{H}}^{(1+j)}}\frac{d}{dn}\left(\bar{\mathscr{H}}^{(1+j)}\lambda\frac{d\bar{T}}{dn}\right)+\sum_{k\in\mathscr{K}}\bar{\rho}\bar{Y}_k\bar{V}_k c_{pk}\frac{d\bar{T}}{dn}+\sum_{k\in\mathscr{K}}h_k W_k\omega_k=0. \tag{13}$$

One may notice that Eq. (10) indicates that the first term in the pressure series expansion $\bar{p}$ is constant along the stagnation streamline.

2.3. *Boundary Conditions*

The boundary conditions at the shock are provided by the Rankine–Hugoniot relations. The shock location is denoted by $\sigma(s)$, so that at $n=\sigma(s)$ the following relations express the conservation of mass, tangential and normal momentum, energy, and species

$$\rho(s,\sigma(s))(-u(s,\sigma(s))\sin\theta+v(s,\sigma(s))\cos\theta)=\rho_\infty v_\infty\sin(\alpha+\theta), \tag{15}$$

$$u(s,\sigma(s))\cos\theta+v(s,\sigma(s))\sin\theta=-v_\infty\cos(\alpha+\theta), \tag{16}$$

$$\rho(s,\sigma(s))(-u(s,\sigma(s))\sin\theta+v(s,\sigma(s))\cos\theta)^2+p(s,\sigma(s))=\rho_\infty v_\infty^2\sin^2(\alpha+\theta)+p_\infty, \tag{17}$$

$$\tfrac{1}{2}(-u(s,\sigma))\sin\theta+v(s,\sigma(s))\cos\theta)^2+h(s,\sigma(s))=\tfrac{1}{2}v_\infty^2\sin^2(\alpha+\theta)+h_\infty, \tag{18}$$

$$Y_k(s,\sigma(s))=Y_{k,\infty},\qquad k\in\mathscr{K}, \tag{19}$$

where the subscript ∞ refers to the uniform state in front of the shock, h is the enthalpy of the mixture and $\rho_\infty, v_\infty, p_\infty$, and h_∞ denote respectively the density, pressure, normal velocity, and enthalpy of air in front of the shock. In these relations α designates the angle between the tangent to the body surface and the axis of symmetry and θ is the angle between the tangent to the body surface and the tangent to the shock (see Fig. 1), i.e.,

$$\cos\theta=\frac{1+\kappa\sigma}{((1+\kappa\sigma)^2+(d\sigma/ds)^2)^{1/2}},\qquad \sin\theta=\frac{(d\sigma/ds)}{((1+\kappa\sigma)^2+(d\sigma/ds)^2)^{1/2}}. \tag{20}$$

Note that the chemistry is assumed to be frozen through the shock. Mixed boundary conditions could also be used as described in Ref. [4]. Equations (15)–(19) written at $s=0$ then yield the following relations at the shock $\bar{\sigma}=\sigma(0)$:

$$\bar{\rho}(\bar{\sigma})\,\bar{v}(\sigma)=\rho_\infty v_\infty, \tag{21}$$

$$\bar{\rho}(\bar{\sigma})\,\bar{v}^2(\bar{\sigma})+\bar{p}(\sigma)=\rho_\infty v_\infty^2+p_\infty, \tag{22}$$

$$\tfrac{1}{2}\bar{v}^2(\sigma)+\bar{h}(\bar{\sigma})=\tfrac{1}{2}v_\infty^2+h_\infty, \tag{23}$$

$$\bar{Y}_k(\bar{\sigma})=Y_{k,\infty},\qquad k\in\mathscr{K}. \tag{24}$$

By specifying the state law and the thermodynamic expressions for the enthalpy of the mixture h, these equations can be solved to provide the values, at the shock, of $\bar{\rho}$, $\bar{v}$, $\bar{p}$, and $\bar{T}$. These values will be denoted $\bar{\rho}_{\bar{\sigma}}$, $\bar{v}_{\bar{\sigma}}$, $\bar{p}_{\bar{\sigma}}$, and $\bar{T}_{\bar{\sigma}}$, respectively, in the following development.

To obtain a complete set of boundary conditions, expressions for $\tilde{u}$ and $\tilde{p}$ have to be determined. Davis [4] has shown that the expansion of the boundary conditions (15)–(19) around $s=0$ only provides elliptic relations, i.e., that $\tilde{u}$ and $\tilde{p}$ appear as functions of $\tilde{\sigma}$ which is not known until the shock is determined downstream in the vicinity of the stagnation streamline. To start the iteration process, Davis assumed that

$$\frac{d\sigma}{ds}(s)=0. \tag{25}$$

According to (20), this implies that $\cos\theta=1$ and $\sin\theta=0$, and consequently that $\theta(s)=0$, so that the body surface and the shock are locally concentric. The matching conditions at the shock then become

$$\rho(s,\sigma(s))\,v(s,\sigma(s))=\rho_\infty v_\infty\sin\alpha, \tag{26}$$

$$u(s,\sigma(s))=-v_\infty\cos\alpha, \tag{27}$$

$$\rho(s,\sigma(s))\,v^2(s,\sigma(s))+p(s,\sigma(s))=\rho_\infty v_\infty^2\sin^2\alpha+p_\infty, \tag{28}$$

$$\tfrac{1}{2}v^2(s,\sigma(s))+h(s,\sigma(s))=\tfrac{1}{2}v_\infty^2\sin^2\alpha+h_\infty, \tag{29}$$

$$Y_k(s,\sigma(s))=Y_{k,\infty},\qquad k\in\mathscr{K}. \tag{30}$$

These relations replace the general expressions (15)–(19). It may be shown that they also lead to Eqs. (21)–(24) on the stagnation streamline.

From Eqs. (26)–(30) and using the fact that $(d^2\sigma/ds^2)(s)=0$, one finds that

$$\tilde{u}(\tilde{\sigma})=-\kappa v_\infty, \tag{31}$$

$$\left[1+\frac{c_p\bar{T}_{\tilde{\sigma}}}{\tilde{v}_{\tilde{\sigma}}^2}-\frac{c_pT_\infty\rho_\infty}{p_\infty}\right]\tilde{p}(\tilde{\sigma})=-\frac{\kappa^2v_\infty}{2}\left[\rho_\infty\tilde{v}_{\tilde{\sigma}}-\tilde{\rho}_{\tilde{\sigma}}v_\infty-2\rho_\infty\times\left(1+\frac{c_p\bar{T}_{\tilde{\sigma}}}{\tilde{v}_{\tilde{\sigma}}^2}\right)(\tilde{v}_{\tilde{\sigma}}-v_\infty)\right]. \tag{32}$$

Note that in the previous assumptions, there is no coupling between the field calculation and the variations of the shock shape. This may lead to significant errors in the shock standoff distance, especially downstream for highly curved bodies like spheres. Davis has shown that this later approximation may be removed with successive iterations

[4]. However, it appears more adequate to take into account the shock shape variations even in the TVSL calculations and derive new relations at the shock. By performing an order of magnitude analysis, we find that

$$\cos\theta \sim 1, \qquad \sin\theta \sim \frac{d\sigma}{ds} \sim \varepsilon, \tag{33}$$

and, keeping terms up to first order ($\sim$TVSL approximation) in the Rankine–Hugoniot conditions (15)–(19), we obtain the following set of simplified expressions:

$$\rho(s,\sigma(s))\left(-u(s,\sigma(s))\frac{d\sigma}{ds}+v(s,\sigma(s))\right) = \rho_\infty v_\infty \sin\alpha, \tag{34}$$

$$u(s,\sigma(s)) = -v_\infty \cos\alpha, \tag{35}$$

$$p(s,\sigma(s)) = \rho_\infty v_\infty^2 \sin^2\alpha, \tag{36}$$

$$h(s,\sigma(s)) = \tfrac{1}{2} v_\infty^2 \sin^2\alpha, \tag{37}$$

$$Y_k(s,\sigma(s)) = Y_{k,\infty}, \qquad k\in\mathscr{K}. \tag{38}$$

By expanding these relations around $s=0$, it is then found that

$$\bar\rho(\sigma)\,\bar v(\bar\sigma) = \rho_\infty v_\infty, \tag{39}$$

$$\bar p(\bar\sigma) = \rho_\infty v_\infty^2, \tag{40}$$

$$\bar h(\bar\sigma) = \tfrac{1}{2} v_\infty^2, \tag{41}$$

$$\bar Y_k(\bar\sigma) = Y_{k,\infty}, \qquad k\in\mathscr{K}, \tag{42}$$

$$\bar u(\bar\sigma) = -\kappa v_\infty, \tag{43}$$

$$\tilde p(\bar\sigma) = -\rho_\infty \kappa^2 v_\infty^2. \tag{44}$$

The values of $\bar u$ and $\tilde p$ at the shock will be denoted $\bar u_{\bar\sigma}$ and $\tilde p_{\bar\sigma}$ in the following. Expressions (39)–(44) and (34)–(38) constitute a new set of conditions at the shock for the modified TVSL approximation. When used in place of the classical conditions (21)–(24), (31)–(32), and (26)–(30), they yield an improved thin viscous shock layer solution.

The boundary conditions at the body surface may also require a careful analysis if one wishes to describe catalytic effects. For simplicity we consider that a no-slip condition determines the velocity components, that the temperature of the surface is specified, and that the mixture close to the surface is in chemical equilibrium. The corresponding conditions are

$$v(s,0) = 0, \tag{45}$$

$$u(s,0) = 0, \tag{46}$$

$$Y_k(s,0) = Y_{k,w}, \qquad k\in\mathscr{K}, \tag{47}$$

$$T(s,0) = T_w, \tag{48}$$

where T_w denotes the body wall temperature and $Y_{k,w}$ is the air equilibrium mass fraction at T_w. On the stagnation streamline, one obtains

$$\bar v(0) = 0, \tag{49}$$

$$\bar u(0) = 0, \tag{50}$$

$$\bar Y_k(0) = Y_{k,w}, \qquad k\in\mathscr{K}, \tag{51}$$

$$\bar T(0) = T_w. \tag{52}$$

At this stage one may note that there are two boundary conditions for the normal velocity $v(s,\sigma(s))$ (or $\bar v$), although Eq. (1) (or (8)) is only first order. The extra boundary condition $v = v_\sigma$ (or $\bar v = \bar v_{\bar\sigma}$) will indeed determine the shock location σ (or $\bar\sigma$).

2.4. *Thermodynamics and Chemistry*

The equation of state is written in the form

$$\rho = pW/RT, \tag{53}$$

where $1/W = \sum_{k\in\mathscr{K}} Y_k/W_k$ is the molecular weight of the mixture and R is the universal gas constant. Species thermodynamic properties like c_{pk} or h_k are estimated from polynomial fits of Baulknight's data [17] and the mixture constant pressure heat capacity c_p and enthalpy h are given by

$$c_p = \sum_{k\in\mathscr{K}} Y_k c_{pk}, \qquad h = \int_{T^0}^{T} c_p(T')\,dT' + \sum_{k\in\mathscr{K}} Y_k h_k(T^0). \tag{54}$$

We also consider I elementary reversible reactions involving K chemical species

$$\sum_{k\in\mathscr{K}} \nu'_{ki}\mathscr{X}_k \rightleftharpoons \sum_{k\in\mathscr{K}} \nu''_{ki}\mathscr{X}_k, \qquad i\in\mathscr{I}, \tag{55}$$

where $\mathscr{I}$ is the set of reaction indices, $\mathscr{X}_k$ is the symbol of the kth species, and ν'_{ki} and ν''_{ki} are the soichiometric coefficients. The production rate of the kth species can then be written as

$$\omega_k = \sum_{i\in\mathscr{I}} (\nu''_{ki} - \nu'_{ki})\,q_i, \qquad q_i = \mathscr{C}_{fi}\prod_{k\in\mathscr{K}} [\mathscr{X}_k]^{\nu'_{ki}} - \mathscr{C}_{ri}\prod_{k\in\mathscr{K}} [\mathscr{X}_k]^{\nu''_{ki}}, \tag{56}$$

where q_i is the rate of progress variable of the ith reaction and appears as the difference between the forward and reverse rates, $[\mathscr{X}_k]$ is the molar concentration of the kth

species, and $\mathscr{C}_{fi}$ and $\mathscr{C}_{ri}$ are the forward and reverse rate constants of the ith reaction. Denoting X_k the mole fraction of the kth species, the quantities X_k, Y_k, and $[\mathscr{X}_k]$ are related by $X_k = Y_k W/W_k$ and $[\mathscr{X}_k] = pX_k/RT$, where $W = \sum_{k=1}^{K} X_k W_k$. The forward and reverse rate constants for the ith reaction are taken in the form $\mathscr{C}_{fi} = A_i T^{\beta_i} \exp(-E_i/RT)$ and $\mathscr{C}_{ri} = \mathscr{C}_{fi}/\mathscr{C}_{ei}$, where A_i is the pre-exponential factor, β_i is the temperature exponent, E_i is the activation energy, and $\mathscr{C}_{ei}$ is the equilibrium constant of the ith reaction. In some reactions an arbitrary third body, usually denoted M, is required for the reaction to proceed. In this situation the rate of progress q_i must be multiplied by an effective third body concentration $ctb_i = \sum_{k \in \mathscr{K}} \alpha_{ki} [\mathscr{X}_k]$, where the α_{ki} are one if all the species contribute equally as third bodies [18].

2.5. *Transport Properties*

A simplified transport algorithm is adopted in the present paper. The normal component of the diffusion velocity is divided into two parts

$$V_k = \mathscr{V}_k + V_m, \tag{57}$$

where

$$\mathscr{V}_k = -D_k \frac{d}{dn} \log X_k \tag{58}$$

and

$$D_k = (1 - Y_k) \Big/ \sum_{l \neq k} (X_l/\mathscr{D}_{kl}). \tag{59}$$

In these expressions $\mathscr{V}_k$ is the diffusion velocity due to species gradients and is evaluated with the Hirschfelder–Curtiss approximation and $\mathscr{D}_{kl}$ is the binary diffusion coefficient for the species pair (k, l). The velocity V_m is a correction velocity included to ensure that the mass is conserved $V_m = -\sum_{k \in \mathscr{K}} Y_k \mathscr{V}_k$ [19]. It has been shown in Ref. [20] that these diffusion velocities are accurate approximations of those exactly obtained by inverting the Stefan–Maxwell equations. The transport coefficients η, λ, and $\mathscr{D}_{kl}$ are finally expressed in terms of the state variables p, T, Y_k, $k \in \mathscr{K}$, and molecular parameters. The corresponding formulas may be found in Ref. [19]. Note that ambipolar diffusion is used to determine the diffusion coefficients for ionic species.

3. NUMERICAL METHOD

We have seen in the previous sections that on the stagnation streamline the thin viscous shock layer equations reduce to a two-point boundary value problem with a free boundary. The unknown function $\mathscr{X}$ has the components $\mathscr{X} = (\bar{v}, \bar{u}, \tilde{p}, \bar{T}, \bar{Y}_1, \ldots, \bar{Y}_K)$ and is defined on the unknown interval $[0, \bar{\sigma}]$. A simplified system of equations modeling a perfect gas and derived from (8)–(13), (39)–(44), and (49)–(52) is investigated in Ref. [21] from a mathematical point of view and the existence of a solution is established. The first step of the numerical method is to transform the free boundary value problem into a nonlinear eigenvalue problem by introducing the transformed coordinate [22]

$$\xi = n/\bar{\sigma}. \tag{60}$$

This transformation is suggested by other studies of free boundary value problems (see Ref. [22]). The same technique is also useful in theoretical investigations like those of Refs. [21], [23]. An alternative approach could be to use invariant embedding techniques and Riccati type equations [24]. A problem arising from the introduction of the enlarged unknown $(\mathscr{X}, \bar{\sigma})$, however, is that the corresponding discrete equations are no longer in block-tridiagonal form. To remove this difficulty, a classical procedure consists in considering $\bar{\sigma}$ as a function of ξ and adding the dummy equation

$$\frac{d\bar{\sigma}}{d\xi} = 0. \tag{61}$$

This procedure is rather standard and it is adopted, for example, in Ref. [25] to construct an adaptive continuation procedure for flame calculations. We thus consider a new unknown function $\mathscr{X} = (\bar{v}, \bar{u}, \tilde{p}, \bar{T}, \bar{Y}_1, \ldots, \bar{Y}_K, \bar{\sigma})$ defined on the unit interval $[0, 1]$. Introducing the operator

$$\mathscr{E} = \begin{bmatrix} \dfrac{1+j}{\bar{\mathscr{H}}} \rho\bar{u} + \dfrac{1}{\bar{\mathscr{H}}^{(1+j)}\bar{\sigma}} \dfrac{d}{d\xi} (\bar{\mathscr{H}}^{(1+j)} \bar{\rho}\bar{v}) \\ \dfrac{1}{\bar{\mathscr{H}}} \bar{\rho}\bar{u}^2 + \dfrac{\bar{\rho}\bar{v}}{\bar{\sigma}} \dfrac{d\bar{u}}{d\xi} + \dfrac{\bar{\rho}\kappa u\bar{v}}{\bar{\mathscr{H}}} + \dfrac{2}{\bar{\mathscr{H}}} \tilde{p} \\ \quad - \dfrac{1}{\bar{\mathscr{H}}^{(2+j)}\bar{\sigma}} \dfrac{d}{d\xi} \left(\bar{\mathscr{H}}^{(2+j)} \eta \left(\dfrac{1}{\bar{\sigma}} \dfrac{d\bar{u}}{d\xi} - \dfrac{\kappa\bar{u}}{\bar{\mathscr{H}}} \right) \right) \\ \quad - \dfrac{\bar{\rho}\kappa\bar{u}^2}{\bar{\mathscr{H}}} + \dfrac{1}{\bar{\sigma}} \dfrac{d\tilde{p}}{d\xi} \\ \cdots\cdots\cdots\cdots\cdots\cdots\cdots\cdots\cdots\cdots \\ \dfrac{\bar{\rho}\bar{v}}{\bar{\sigma}} \dfrac{d\bar{Y}_k}{d\xi} - W_k \omega_k + \dfrac{1}{\bar{\mathscr{H}}^{(1+j)}\bar{\sigma}} \dfrac{d}{d\xi} (\bar{\mathscr{H}}^{(1+j)} \bar{\rho} \bar{Y}_k \bar{V}_k) \\ \cdots\cdots\cdots\cdots\cdots\cdots\cdots\cdots\cdots\cdots \\ \dfrac{\bar{\rho}\bar{v}\bar{c}_p}{\bar{\sigma}} \dfrac{d\bar{T}}{d\xi} - \dfrac{1}{\bar{\mathscr{H}}^{(1+j)}\bar{\sigma}^2} \dfrac{d}{d\xi} \left(\bar{\mathscr{H}}^{(1+j)} \lambda \dfrac{d\bar{T}}{d\xi} \right) \\ \quad + \sum_{k \in \mathscr{K}} \dfrac{\bar{\rho} \bar{Y}_k \bar{V}_k c_{pk}}{\bar{\sigma}} \dfrac{d\bar{T}}{d\xi} + \sum_{k \in \mathscr{K}} h_k W_k \omega_k \\ \dfrac{d\bar{\sigma}}{d\xi} \end{bmatrix}, \tag{62}$$

where the dotted lines stand for the species equations, and the corresponding boundary operators

$$\mathscr{B}_0 = \begin{bmatrix} \bar{v} \\ \bar{u} \\ -\dfrac{\bar{\rho}\kappa\bar{u}^2}{\bar{\mathscr{H}}} + \dfrac{1}{\bar{\sigma}}\dfrac{d\bar{p}}{d\xi} \\ \cdots\cdots\cdots \\ \bar{Y}_k - Y_{k,w} \\ \cdots\cdots\cdots \\ \bar{T} - T_w \\ \dfrac{d\bar{\sigma}}{d\xi} \end{bmatrix}, \tag{63}$$

$$\mathscr{B}_1 = \begin{bmatrix} \dfrac{1+j}{\bar{\mathscr{H}}}\rho\bar{u} + \dfrac{1}{\bar{\mathscr{H}}^{(1+j)}\bar{\sigma}}\dfrac{d}{d\xi}(\bar{\mathscr{H}}^{(1+j)}\bar{\rho}\bar{v}) \\ \bar{u} - \tilde{u}_{\bar{\sigma}} \\ \tilde{p} - \tilde{p}_{\bar{\sigma}} \\ \cdots\cdots\cdots \\ \bar{Y}_k - Y_{k,\infty} \\ \cdots\cdots\cdots \\ T - T_{\bar{\sigma}} \\ \bar{v} - \bar{v}_{\bar{\sigma}} \end{bmatrix}, \tag{63}$$

where $\mathscr{B}_0$ and $\mathscr{B}_1$ are evaluated at $\xi = 0$ and $\xi = 1$, respectively, we must solve the two point boundary value problem $(\mathscr{B}_0, \mathscr{E}, \mathscr{B}_1)(\mathscr{X}) = 0$. Note that the extra boundary condition for the normal velocity $\bar{v}$ is used as a "boundary condition" for the eigenvalue $\bar{\sigma}$. With the continuous differential operators replaced by difference expressions, we seek a discrete approximation X_Ξ of $\mathscr{X}$ on a mesh Ξ [11],

$$\Xi = \{0 = \xi_1 < \xi_2 < \cdots < \xi_M = 1\}, \tag{64}$$

solution of a nonlinear system of difference equations

$$F_\Xi(X_\Xi) = 0, \tag{65}$$

where F_Ξ denote the discrete equations and M is the number of grid points. For an initial solution estimate X^0 that is sufficiently close to X_Ξ, the system of equations in (65) can be solved by Newton's method. We write

$$J(X^n)(X^{n+1} - X^n) = -\lambda_n F(X^n), \qquad n = 0, 1, \ldots, \tag{66}$$

where X^n denotes the nth iterate, λ_n is the nth damping parameter, $0 < \lambda_n \leqslant 1$, which should be chosen to ensure a reduction in the size of the Newton corrections at each iteration [12], and J is the Jacobian matrix. The Jacobian matrix is obtained by finite differences and subroutine libraries are used to handle chemistry and transport properties [14, 18, 19, 26]. A system of linear block tridiagonal equations must be solved at each iteration for corrections to the previous solution vector. In practice, a modified Newton's method is employed in which the Jacobian is re-evaluated periodically [27]. We terminate the Newton iteration when

$$\|X^{n+1} - X^n\|_2 = \|J^{-1}(X^n)\, F(X^n)\|_2 < \mathrm{TOL} \tag{67}$$

where we typically take $\mathrm{TOL} = 10^{-5}$.

It has been shown by Deuflhard [12] that the scaling by the inverse of the Jacobian of the function residuals is better suited to Newton's method and is affine invariant. The previous criterion has been used extensively in flame problems (see Ref. [14]) and guarantees the accuracy of the solution on the given grid Ξ. To assure that the converged discrete solution correctly represents the continuous solution, the grid is adaptively densified. This consists in successively refining the grids in such a way that for the final grid Ξ we have

$$\int_{\xi_m}^{\xi_{m+1}} \left|\frac{d\omega_l}{d\xi}\right| d\xi \leqslant \varepsilon_l \Big(\sup_{0 \leqslant \xi \leqslant 1} \omega_l - \inf_{0 \leqslant \xi \leqslant 1} \omega_l \Big),$$
$$m = 0, 1, \ldots, M-1, \; l \in \mathscr{L}, \tag{68}$$

where ω_l, $l \in \mathscr{L}$, is a family of weights and ε_l, $l \in \mathscr{L}$, are small numbers, less than one. The family of weights is usually formed by the gradients and second derivatives of each component of the solution vector and of mesh regularity weights as explained in Refs. [13, 15, 25, 27].

One of the advantages of Newton's method is the fast rate of convergence. A potential problem, however, is that, on each grid, the corresponding starting estimates must be in the domain of convergence of the method. In order to suppress this sensitivity to starting estimates and to bring these estimates into the domain of convergence of Newton's method, pseudo-unsteady fully implicit iterations are used. Unsteady terms are only appended to the species and energy equations which then take the form

$$\bar{\rho}\frac{\partial \bar{Y}_k}{\partial t} + \frac{\bar{\rho}\bar{v}}{\bar{\sigma}}\frac{\partial \bar{Y}_k}{\partial \xi} - W_k\omega_k + \frac{1}{\bar{\mathscr{H}}^{(1+j)}\bar{\sigma}}\frac{\partial}{\partial \xi}(\bar{\mathscr{H}}^{(1+j)}\bar{\rho}\bar{Y}_k\bar{V}_k) = 0, \quad k \in \mathscr{K}, \tag{69}$$

$$\bar{\rho}\bar{c}_p\frac{\partial \bar{T}}{\partial t} + \frac{\bar{\rho}\bar{v}\bar{c}_p}{\bar{\sigma}}\frac{\partial \bar{T}}{\partial \xi} - \frac{1}{\bar{\mathscr{H}}^{(1+j)}\bar{\sigma}^2}\frac{\partial}{\partial \xi}\left(\bar{\mathscr{H}}^{(1+j)}\lambda\frac{\partial \bar{T}}{\partial \xi}\right) + \sum_{k \in \mathscr{K}} \frac{\bar{\rho}\bar{Y}_k\bar{V}_k c_{pk}}{\bar{\sigma}}\frac{\partial \bar{T}}{\partial \xi} + \sum_{k \in \mathscr{K}} h_k W_k \omega_k = 0. \tag{70}$$

No unsteady terms are added to the coupled hydrodynamic–eigenvalue equations.

To obtain the solution at a downstream station ($s > 0$), one has to consider a two-point boundary value problem with first derivatives with respect to the streamwise coordinate s (Eqs. (1)–(6), boundary conditions (34)–(38) and (45)–(48)). The unknown function $\mathscr{X}^s$ has the components $\mathscr{X}^s = (v, u, p, T, Y_1, ..., Y_K)$ and is defined on the unknown interval $[0, \sigma(s)]$. To ensure the continuity of the operators and thus the continuity of the solution (when $s \to 0$) and to ease the initialization of the marching step procedure, it is convenient to introduce transformed coordinates and new dependent variables

$$\zeta = s, \tag{71}$$

$$\xi = n/\sigma(s), \tag{72}$$

$$u = \zeta \bar{u}(\zeta, \xi), \tag{73}$$

$$r = \zeta \bar{\mathscr{R}}(\zeta, \xi), \tag{74}$$

$$p = \bar{p}_{\bar{\sigma}} + \zeta^2 \tilde{p}(\zeta, \xi), \tag{75}$$

We thus consider a new unknown function $\mathscr{X}^\zeta = (v, \bar{u}, \tilde{p}, T, Y_1, ..., Y_K, \sigma)$ defined on the unit interval $[0, 1]$ and we must solve the two-point boundary value problem $(\mathscr{B}_0^\zeta, \mathscr{E}^\zeta, \mathscr{B}_1^\zeta)(\mathscr{X}^\zeta) = 0$. We consider a discretization Σ of the streamwise domain

$$\Sigma = \{0 = \zeta_1 < \zeta_2 < \cdots < \zeta_J = 1\}, \tag{76}$$

and we seek a set of discrete approximations $X_{\underline{\underline{\zeta_j}}}$ of $\mathscr{X}^{\zeta_j}$ at $\zeta = \zeta_j$.

The space marching procedure then consists in solving a succession of discrete problems which can be written

$$F_{\underline{\underline{\zeta_j}}}(X_{\underline{\underline{\zeta_j}}}, X_{\underline{\underline{\zeta_{j-1}}}}) = 0, \qquad j \in \{1, ..., J\}, \tag{77}$$

where $X_{\underline{\underline{\zeta_0}}}$ is the solution on the stagnation streamline. These J problems are solved using fully-implicit finite differences and fully-coupled Newton iterations with the convergence criterion described previously.

No attempt was made to save CPU time by using, for instance, linearized implicit finite differences or freezing the transport coefficients during the Jacobian evaluations or even using the same Jacobian for several steps in the streamwise direction. All these improvements could be implemented easily in the code for repetitive applications. Even in its present form it operates on workstations or minicomputers.

4. NUMERICAL RESULTS

We have applied the numerical method discussed in the previous section to determine the structure of a viscous shock layer at altitude $z = 66$ km for a freestream Mach number of $M_\infty = 19$. The corresponding freestream temperature and pressure, which may be found in tables, are $T_\infty = 235$ K and $p_\infty = 9.7710^{-5}$ atm. The freestream velocity is in this case $v_\infty = 5839$ m/s. A typical value of the body nose radius $1/\kappa = R_0 = 1$ m has been chosen, the wall temperature is taken to be $T_w = 1500$ K, and it is assumed that the body surface is fully catalytic, i.e., that species at the wall are in chemical equilibrium at the wall temperature. An air dissociation reaction mechanism due to Bortner [16] was used and is listed in Table I.

The solution typically requires between 40 to 60 adaptively chosen grid points in the ξ direction. After the grid adaptation the grid points were concentrated near the shock and body surface.

Figure 2 displays the reduced pressure $\tilde{p}/|\tilde{p}_{\bar{\sigma}}|$ and velocity components $\bar{v}/|\bar{v}_{\bar{\sigma}}|$ and $\bar{u}/|\bar{u}_{\bar{\sigma}}|$ profiles. Note that the dependent variables are plotted as functions of $\kappa n = n/R_0$. The corresponding shock values of these variables are found to be $\tilde{p}_{\bar{\sigma}} = -4552$ Pa/m^2, $\bar{u}_{\bar{\sigma}} = 5839$ s^{-1} and $\bar{v}_{\bar{\sigma}} = -693.4$ m/s, and the shock standoff distance is $\bar{\sigma} = 7.24$ cm. The hydrodynamic variables $\tilde{p}$, $\bar{u}$, and $\bar{v}$ present moderate relative changes and, as a consequence, the convergence rate of the method is quite large.

The temperature profile displayed in Fig. 3 exhibits a classical S-shape. It is worth noting that the profile never levels off so that one cannot assume that chemical equilibrium is reached somewhere in the layer. In the first part

TABLE I

Reaction Mecanism for Air Dissociation

	Reaction	A	β	E
1.*f*	$O_2 + M \to O + O + M^a$	3.61E18	−1.0	118.0E03
1.*r*	$O + O + M \to O_2 + M^a$	3.01E15	−0.5	0.0
2.*f*	$N_2 + M \to N + N + M^b$	1.92E17	−0.5	224.7E03
2.*r*	$N + N + M \to N_2 + M^b$	1.09E16	−0.5	0.0
3.*f*	$N_2 + N \to N + N + N$	4.15E22	−1.5	224.7E03
3.*r*	$N + N + N \to N_2 + N$	2.32E21	−1.5	0.0
4.*f*	$NO + M \to N + O + M^c$	3.97E20	−1.5	150.2E03
4.*r*	$N + O + M \to NO + M^c$	1.01E20	−1.5	0.0
5.*f*	$NO + O \to O_2 + N$	3.18E09	+1.0	39.1E03
5.*r*	$O_2 + N \to NO + O$	9.63E11	+0.5	7.152E093
6.*f*	$N_2 + O \to NO + N$	6.75E13	+0.0	74.5E03
6.*r*	$NO + N \to N_2 + O$	1.50E13	+0.0	0.0
7.*f*	$N + O \to NO^+ + e^-$	9.03E09	+0.5	64.37E03
7.*r*	$NO^+ + e^- \to N + O$	1.80E19	−1.0	0.0

Note. Coefficients in the form $k_f = AT^\beta \exp(-E/RT)$. Units are moles, centimeters, seconds, Kelvins, calories/mole.

[a] Third body efficiencies: $\alpha_1(O_2) = 9$, $\alpha_1(O) = 25$; $\alpha_1(N_2) = 2$, $\alpha_1(NO^+) = 0$; $\alpha_1(e^-) = 0$.

[b] Third body efficiencies: $\alpha_2(N_2) = 2.5$, $\alpha_2(N) = 0$; $\alpha_2(NO^+) = 0$, $\alpha_2(e^-) = 0$.

[c] Third body efficiencies: $\alpha_4(O) = 20$, $\alpha_4(N) = 20$; $\alpha_4(NO) = 20$, $\alpha_4(NO^+) = 0$; $\alpha_4(e^-) = 0$.

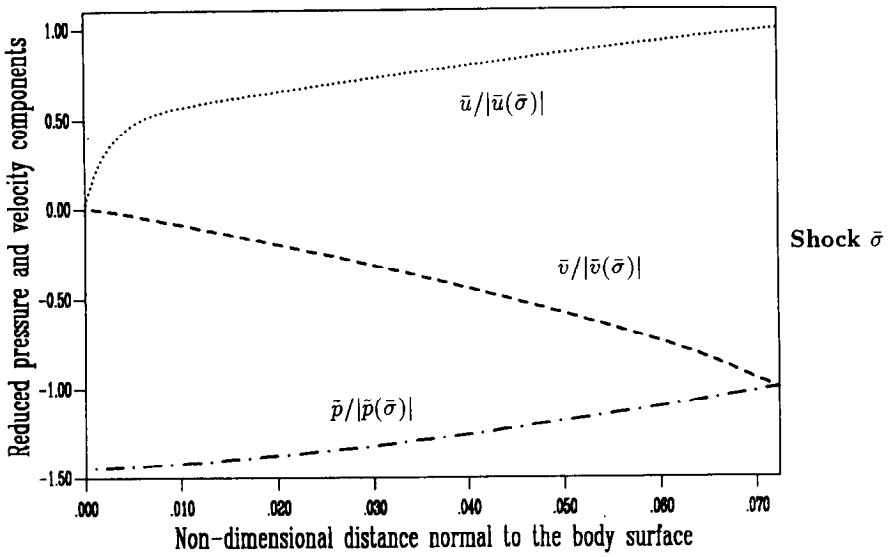

FIG. 2. Reduced pressure $\bar{p}/|\bar{p}(\bar{\sigma})|$ and reduced velocity components $\bar{v}/|\bar{v}(\sigma)|$ and $\bar{u}/|\bar{u}(\sigma)|$ plotted as a function of the reduced coordinate κn on the stagnation streamline.

of the domain, from the shock to approximately the middle of the shock layer, the temperature decreases from $T \approx 12500$ K to $T \approx 7500$ K because of molecular dissociation. In the second part of the domain, in the vicinity of the body surface, the temperature decreases rapidly to the wall temperature.

The species mass fractions are shown in Fig. 4. Strong dissociation of molecular oxygen takes place behind the shock. However, the temperature is not high enough to ensure a complete dissociation of N_2, although there is a noticeable production of atomic nitrogen. Nitrogen oxyde NO is formed with two characteristic peaks. Because the body surface is assumed to be fully catalytic and since the wall temperature is quite low, there is a strong recombination of atoms in the vicinity of the wall, leading to a rapid increase of the O_2 concentration.

On the other hand, Figs. 5–9 display numerical calculations for the same sphere ($R_0 = 1$ m), but corresponding to $z = 75$ km and a larger Mach number, $M_\infty = 25$. The freestream properties are now $T_\infty = 2.4710^{-5}$ atm. The freestream velocity is then $v_\infty = 7181$ m/s. Under these conditions, Fig. 5 displays the shock standoff distance as a

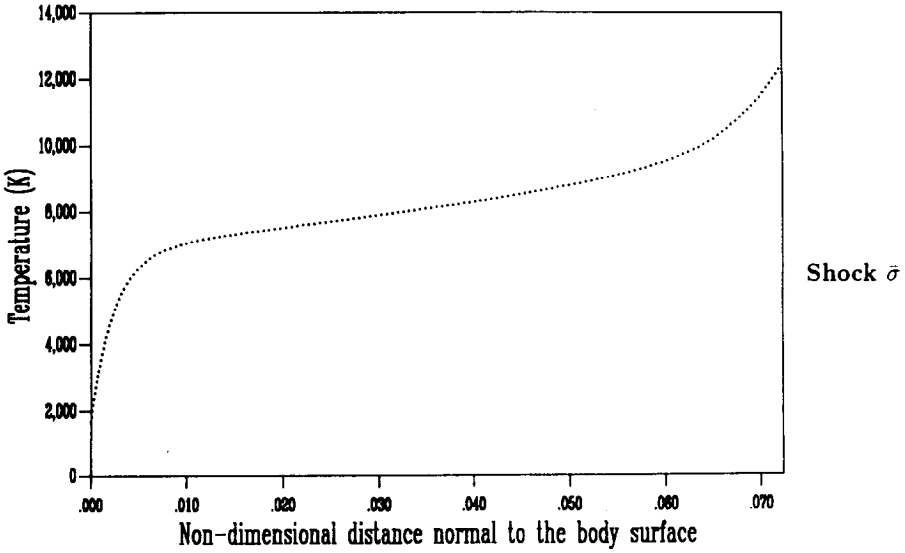

FIG. 3. Temperature profile on the stagnation streamline.

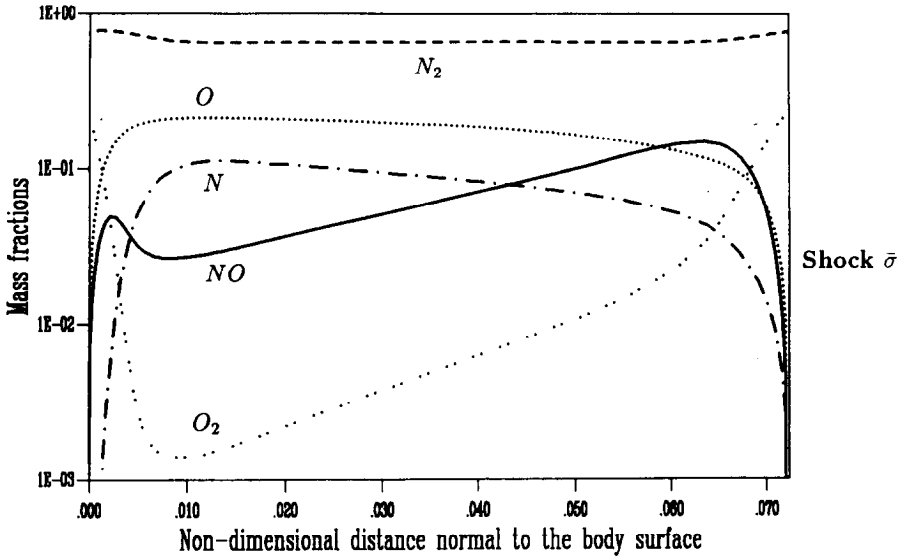

FIG. 4. Species mass fraction profiles on the stagnation streamline.

function of the streamwise coordinate. The present method using modified shock relations (34)–(44) is compared with the TVSL approximation of Davis. A significant discrepancy is observed, especially downstream where the curvature of the body has a strong effect. In this region, Davis' method gives a much greater value of the shock standoff distance.

The difference may be explained as follows. First, one has to remember that the curvature of the sphere keeps a finite (constant) value at each downstream station. As a consequence, the streamlines diverge from the body surface at a certain distance from the stagnation point. The normal component v of the velocity vector will then take positive values across the shock layer. If one now looks at Fig. 6, one notices that even for large values of s, Davies' shock relations yield a negative value for the normal velocity at the shock, v_σ. As the shock standoff distance is adjusted to take into account v_σ, the shock layer width must strongly increase to include a first region, where v is positive, as mentioned previously, and a second region which allows v to reach its negative value at the shock (see Fig. 7). In contrast, the method described in the present paper yields

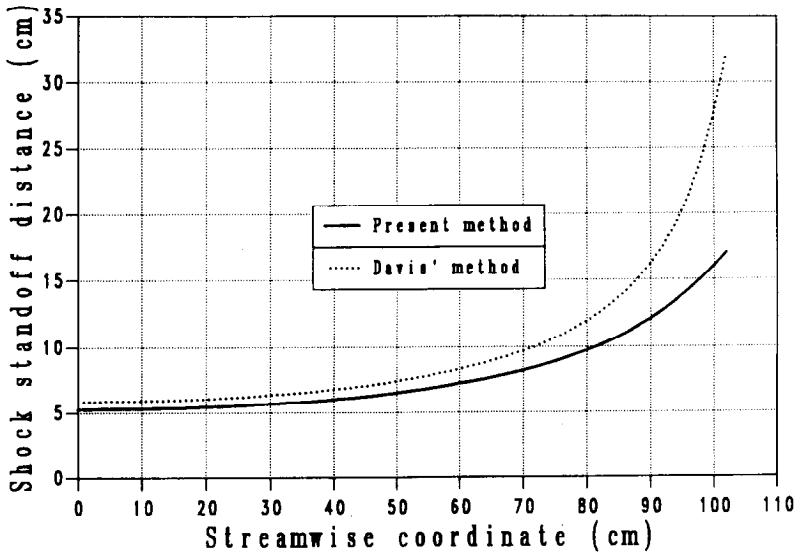

FIG. 5. Shock standoff distance along the sphere. Solid line corresponds to the present shock relations. Broken line is obtained with the standard TVSL shock relations.

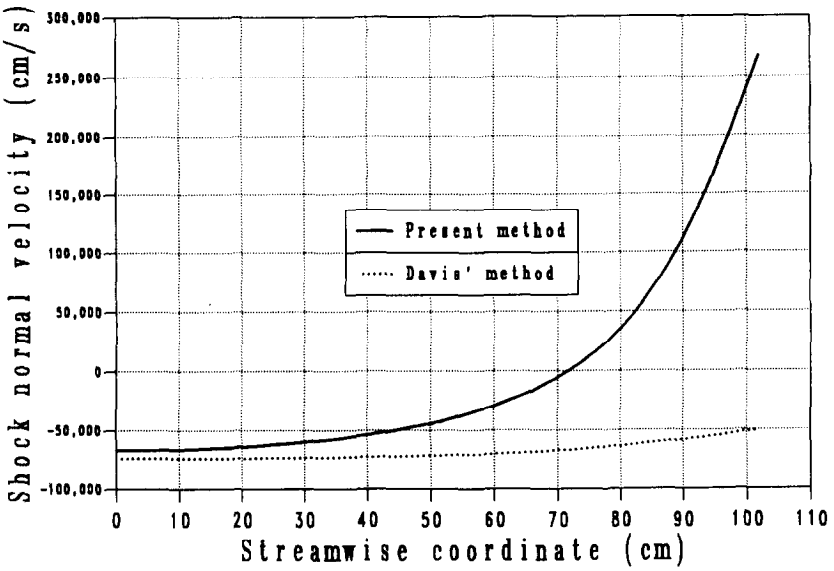

FIG. 6. Velocity component $v(\sigma)$ at the shock, taken in the direction normal to the sphere, plotted as a function of the streamwise coordinate.

positive values of v_σ for large values of s. Positive monotonic normal velocity profiles are generated across the shock layer and a more realistic evolution of the shock shape is obtained. Note again, that another procedure providing improved shock shapes consists in using an Euler code, yielding the shock position along the body and coupling this code to the full VSL calculation as in Ref. [7].

Finally, Figs. 8 and 9 present temperature and electron density profiles along the sphere. The distributions of these quantities diminish monotonically as the streamwise variable increases. This behavior corresponds to the decrease of the shock angle and shock strength in the downstream direction. Of course, this effect is slightly compensated by transport and convection in the streamwise direction.

All the calculations described in this section were performed on an IBM 4381 computer. Typically the convergence on the stagnation line starting from linear profiles requires 50 pseudo-unsteady iterations and 5 to 10 steady iterations. The marching procedure requires less than five steady full or modified Newton iterations at each station. Other configurations have been treated and, in particular,

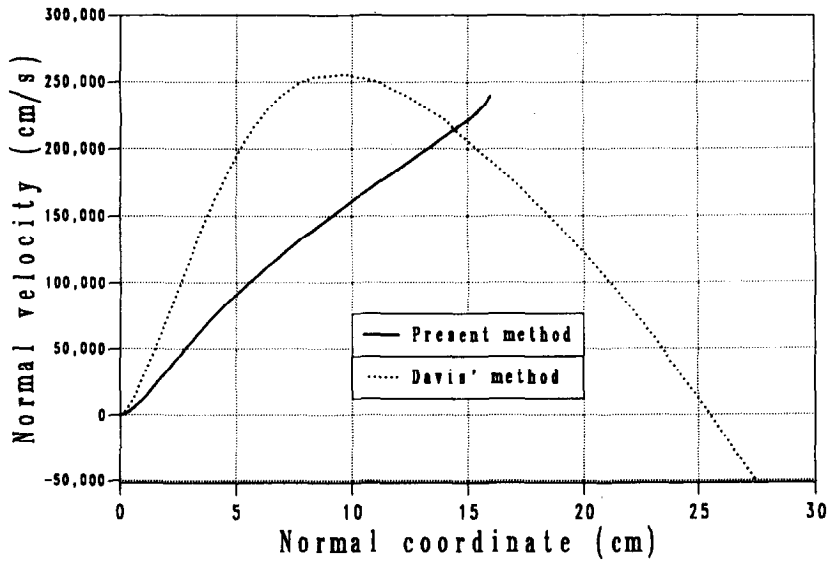

FIG. 7. Profiles of normal velocity plotted in the downstream section $s = 1$ m.

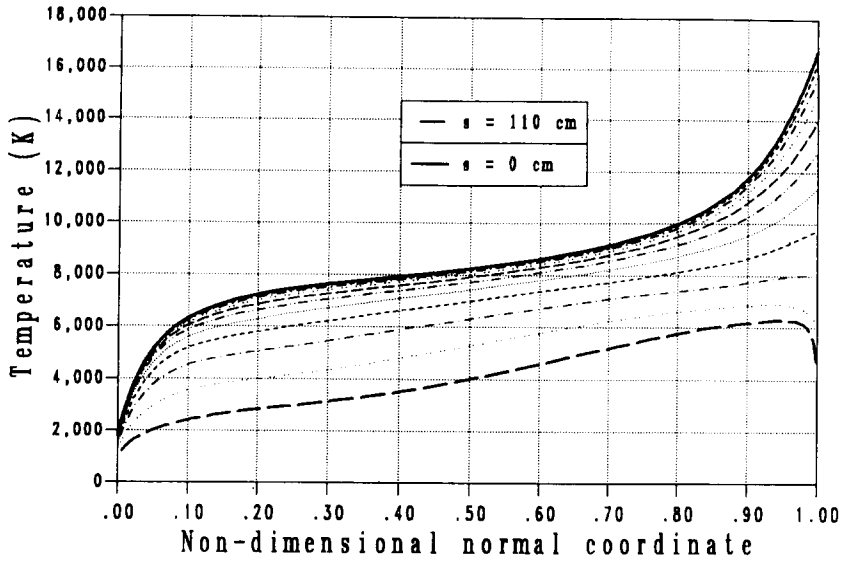

FIG. 8. Temperature profiles plotted in 12 successive stations along the sphere.

hyperbolid shapes of the kind considered by Davis [5]. For such geometries the results obtained by the two methods are quite close. These test calculations, as well as many details, are contained in Ref. [28].

5. CONCLUSION

The viscous shock layer problem of hypersonic flow theory is investigated in this article. This is a free boundary problem as the position of the shock is one of the unknown variables. By introducing a reduced coordinate, the problem is transformed into a nonlinear eigenvalue problem. The resulting two-point boundary value problem is solved using Newton iterations, both steady and unsteady, and adaptive gridding. New boundary conditions are also derived at the shock. These conditions replace the classical thin viscous shock layer relations and lead to an improved calculation of the shape of the shock. This procedure is currently used to investigate more complex systems which include thermodynamic nonequilibrium.

This method which yields simultaneously the flow variables and the shock position has the advantage of coupling all the components of the dependent solution. Block methods of this type are generally faster and more robust than methods which iterate component by component.

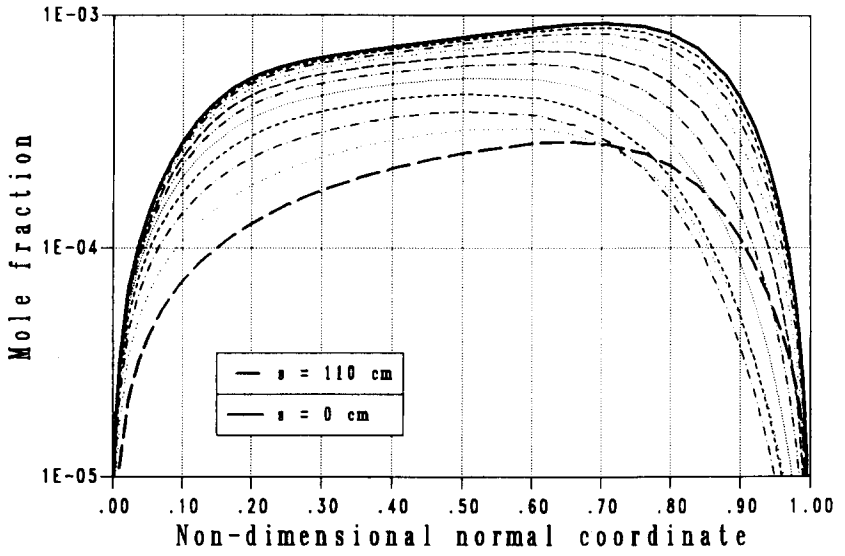

FIG. 9. Electron density profiles plotted in 12 successive stations along the sphere.

ACKNOWLEDGMENT

The authors thank the referee for his many helpful suggestions.

REFERENCES

1. F. G. Blottner, *AIAA J.* **7**, 2281 (1969).
2. W. B. Bush, *J. Fluid Mech.* **20**, 353 (1964).
3. R. T. Davis and I. Flügge-Lotz, *J. Fluid Mech.* **20**, 593 (1964).
4. R. T. Davis, *AIAA J.* **8**, 843 (1970).
5. R. T. Davis, AIAA Paper 70-805, Los Angeles, CA, 1970 (unpublished).
6. A. L. Murray and C. H. Lewis, *AIAA J.* **16**, 1279 (1978).
7. D. J. Song, S. Swaminathan, and C. H. Lewis, *J. Spacecr. Rockets* **22**, 614 (1985).
8. C. D. Scott, "Catalytic Recombination of Nitrogen and Oxygen on High Temperature Reusable Surface Insulation," in *Aerothermodynamics and Planetary Entry*, Progress in Astronautics and Aeronautics, Vol. 77, edited by A. L. Crosbie (Am. Inst. Aeronaut. Astronaut., New York, 1981).
9. D. A. Anderson, J. C. Tannehill, and R. H. Pletcher, *Computational Fluid Mechanics and Heat Transfer* (Hemisphere, New York, 1984).
10. J. D. Waskiewicz, A. L. Murray, and C. H. Lewis, *AIAA J.* **16**, 189 (1978).
11. E. L. Allgower, K. Böhmer, F. A. Potra, and W. C. Rheinboldt, *SIAM J. Numer. Anal.* **23**, 160 (1986).
12. P. Deuflhard, *Numer. Math.* **22**, 289 (1974).
14. M. D. Smooke, *J. Comput. Phys.* **48**, 72 (1982).
15. R. D. Russell and J. Christiansen, *SIAM J. Numer. Anal.* **15**, 59 (1978).
16. M. H. Bortner, *AMRC Proc.* **14**, Part 1 (1966).
17. C. W. Baulknight, in *Proceedings, 2nd conference on Kinetics, Equilibria and Performance of High-Temperature Systems, The Combustion Institute, Los Angeles, CA, 1962* (unpublished).
18. R. J. Kee, J. A. Miller, and T. H. Jefferson, "CHEMKIN: A General-Purpose, Problem-Independent, Transportable, Fortran Chemical Kinetics Code Package," SAND80-8003, SANDIA National Laboratories, 1983.
19. R. J. Kee, J. Warnatz, and J. A. Miller, "A Fortran Computer Code Package for the Evaluation of Gas-Phase Viscosities, Conductivities, and Diffusion Coefficients," SAND83-8209, SANDIA National Laboratories, 1983.
20. V. Giovangigli, *Impact of Computing in Science and Engineering* **3**, 244 (1991).
21. V. Giovangigli, "Mathematical Analysis of Viscous Shock Layer Equations," submitted for publication.
22. G. H. Meyer, "Numerical Methods for Free Boundary Value Problems: 1981 Survey," in *Free Boundary Problems, Theory and Applications, Vol. II*, Research Notes in Mathematics, Vol. 79, edited by A. Fasano and M. Primicerio (Pitman Advanced Publishing Program, Boston, 1983).
23. P. Korman, *SIAM J. Math. Anal.* **19**, 814 (1988).
24. G. H. Meyer, *SIAM J. Numer. Anal.* **18**, 150 (1981).
25. V. Giovangigli and M. D. Smooke, *Appl. Numer. Math.* **5**, 305 (1989).
26. V. Giovangigli and N. Darabiha, "Vector Computers and Complex Chemistry Combustion," in Mathematical Modeling in Combustion and Related Topics, NATO ASI Series, Vol. 140, edited by C. Brauner and C. Schmidt-Laine (Nijhoff, The Hague, 1988).
28. B. Laboudigue, Thesis No. 1990-30, Laboratoire E.M2.C., UPR 288 du CNRS, Ecole Centrale Paris, Chatenay–Malabry, France, 1990.